Solid-State Electronics 201 (2023) 108587

Contents lists available at ScienceDirect

Solid State Electronics

journal homepage: www.elsevier.com/locate/sse

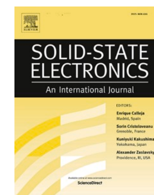

The impact of electron phonon scattering on transport properties of topological insulators: A first principles quantum transport study

Elaheh Akhoundi [a], Michel Houssa [a], Aryan Afzalian [b,*]

[a] imec, KU Leuven, Dept. of Physics and Astronomy, Leuven, Belgium
[b] imec, Leuven, Belgium

ARTICLE INFO

The review of this paper was arranged by "Francisco Gamiz"

Keywords:
Semiconductor device modelling
Topological insulators
2D materials
NEGF

ABSTRACT

Using first-principles calculations and non-equilibrium Green's function, we study the topologically-protected carrier transport in the edges of topological insulator ribbons. We investigate the effects of electron–phonon interactions on the edge state transport. We observed that in topological insulator with small bulk gaps, electron–phonon scattering results in the bulk states broadening into the bulk gap. This leads to the destruction of the dissipationless transport. However, if the transport is restricted to the protected states, a higher immunity to electron–phonon scattering can be achieved. This can lead to the design of topological insulator field effect transistors operating based on scattering modulation, benefiting from a channel material with strong electron–phonon coupling.

1. Introduction

Topological insulators (TIs) have attracted considerable attention due to their unique properties. 2D topological insulators possess spin-polarized gapless edge states that are robust against elastic backscattering [1,2]. The absence of backscattering is attributed to the bulk electronic structure and time-reversal symmetry. Distinguished by a non-zero Z2 topological invariant, the edge states are protected even when large level of imperfections such as vacancy defects, phonons etc are present [3,4].

The observation of the quantized conductance of the protected states is an essential step in the study of the possible applications of TIs. This has proven to be challenging in the lab and the experimental success has been limited to very low temperature or very short channels [5,6]. This has been attributed to various backscattering mechanisms, such as electron–electron interactions, defects, phonon scattering [7]. Here, we study the effects of electron–phonon coupling on the topologically protected edge conduction using a first principles description and non-equilibrium Green's function (NEGF) formalism implemented in our ATOmistic MOdeling Solver (ATOMOS) [8,9]. Using ATOMOS, we are able to conduct transport simulations on wide TI ribbons, which contain heavy atoms and include spin–orbit coupling effects. To decrease the computational costs, we used a mode-space transformation to reduce the size of the Hamiltonian and overlap matrices [10,11]. In Section 2, we summarize the computational methods used in our simulations. We discuss the results in Section 3 and draw conclusions in Section 4.

2. Method

ATOMOS operates in a NEGF framework. Density functional theory (DFT) simulations are carried out to compute the electronic properties of a material, including Hamiltonian matrix elements. Here we focus on two widely studied topological insulators, stanene and bismuthene. The former has a small bulk gap of 0.17 eV [12] while the latter possess a larger bulk gap of 0.5 eV [4]. By choosing these two materials, we can compare the impact of electron–phonon interactions on protected and non-protected states.

The OpenMX package [13,14] is used to perform the DFT simulations and to extract the matrix elements. The generalized gradient approximation (GGA) implementation of DFT with the Perdew-Burke-Ernzerhof (PBE) exchange–correlation (XC) functional is employed. The Brillouin zone was sampled by a 16x1x1 Monkhorst-Pack grid. All the structures are fully relaxed with atomic force convergence criterion of 10^{-3} eV/Å. A vacuum of 15 Å is introduced in the non-periodic directions. The spin–orbit coupling effects are included. The temperature is set at 300 K in all the simulations. We have obtained non-zero Z2 invariant for the monolayers (2D) of stanene and bismuthene. Additionally, the possible edge-to-edge tunneling is included in our model through the use of

* Corresponding author.
E-mail addresses: elaheh.akhoundi@imec.be (E. Akhoundi), michel.houssa@imec.be (M. Houssa), aryan.afzalian@imec.be (A. Afzalian).

https://doi.org/10.1016/j.sse.2022.108587

Available online 2 January 2023
0038-1101/© 2023 Elsevier Ltd. All rights reserved.

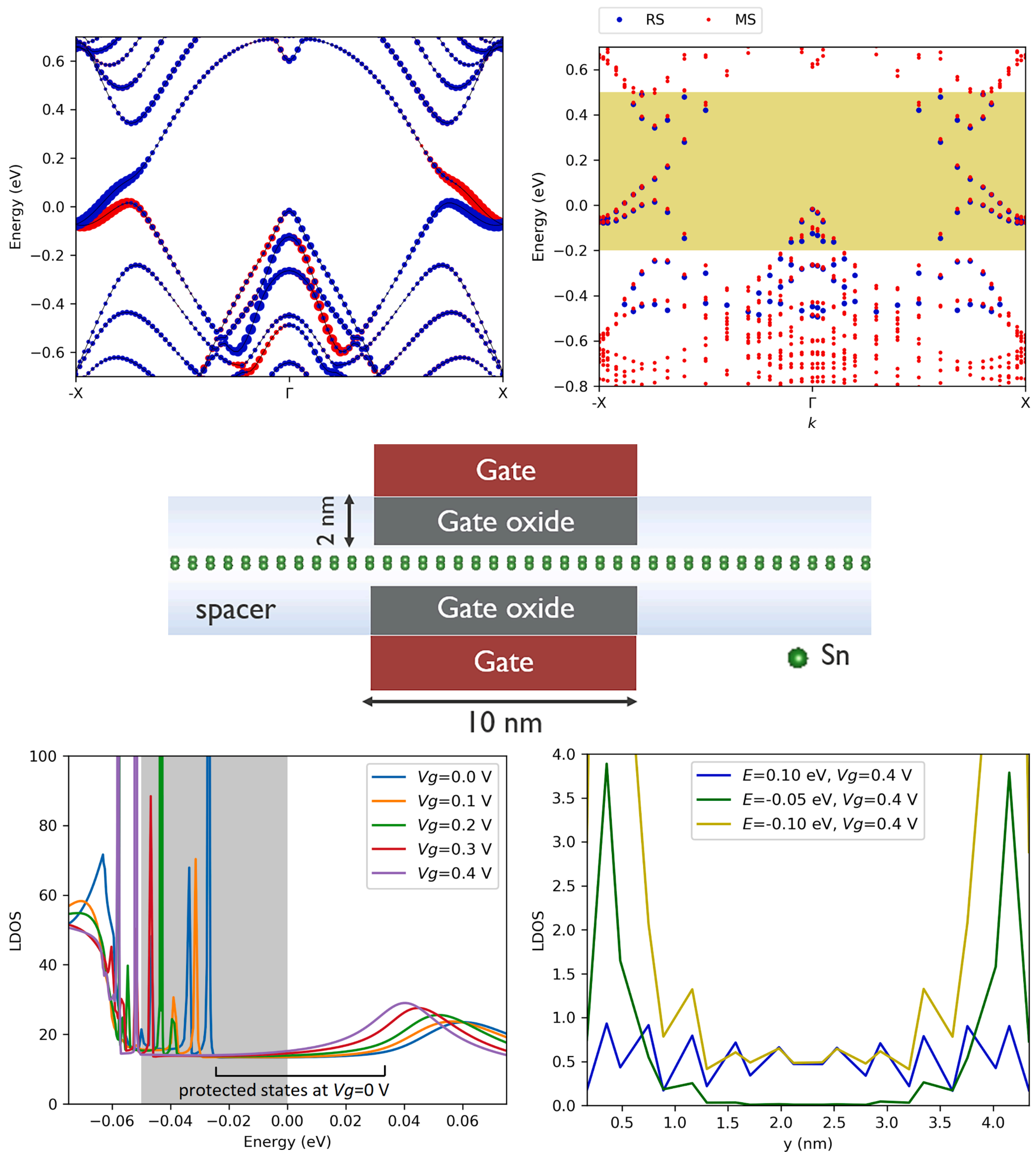

Fig. 1. (a) The spin-resolved band structure projected on the edge atoms obtained for a 4 nm wide zigzag stanene nanoribbon with Fluorine edge passivation. Blue dots show spin-up states and red dots represent the spin-down states. (b) The band structure calculated by the original (RS) and mode-space (MS) Hamiltonians. The shaded area shows the energy window of interest. (c) The sketch of the device structure under study (d) the calculated LDoS for different gate voltages. The shaded area exhibits the Fermi window. (e) LDoS across the width of the ribbon at various energies obtained from a ballistic simulation. (f) and(g): same as (e) and(d) for various deformation potentials. (h) IV curves for the ballistic limit as well as the dissipative case with a deformation potential of 16 eV. (For interpretation of the references to colour in this figure legend, the reader is referred to the web version of this article.)

atomistic (first-principles) Hamiltonian.

The Hamiltonian and overlap matrix elements are imported to ATOMOS. The Hamiltonian matrix for the full device is then constructed. In this work, we study the impact of elastic acoustic phonon scattering on the transport properties of topological insulators, using NEGF and the self-consistent Born approximation with DFT computed effective deformation potential constants [15,16]. The scattering self-energies were directly computed in real-space, by up-converting the

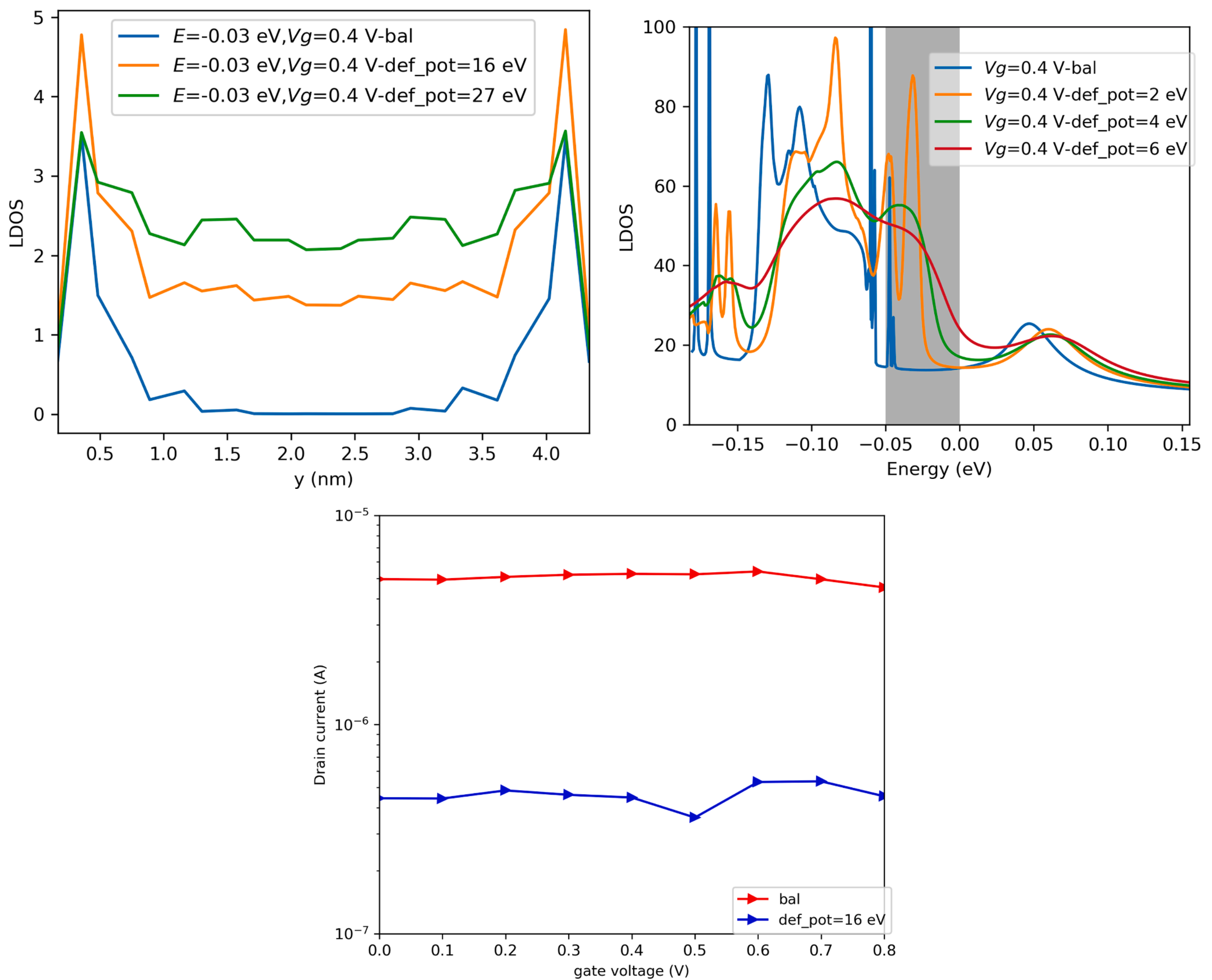

Fig. 1. (*continued*).

mode-space lesser and greater Green's function, and then down-converting to mode-space. It has been shown that the scattering rate of optical phonons is negligible compared to that of acoustic scattering in stanene [17]. The impact of a (weak) optical phonon scattering process is included by considering a small optical deformation constant of 4 eV/nm and a constant phonon energy of 49 meV, values which are fixed in all the simulations performed in this work (except for the ballistic transport simulations). The complete simulation procedure is detailed in [9,18].

3. Results

Fig. 1(a) shows the band structure of a 4 nm wide zigzag stanene ribbon. The spin-resolved contribution of the edge atoms to the band structure is shown as well. The topologically-protected edge states possess a nearly linear dispersion as well as a helical spin texture. The spin texture ensures that intra-edge backscattering is forbidden.

Fig. 1(b) compares the band structure calculated by a real-space Hamiltonian (blue dots) to the band structure computed using a reduced-size, mode-space Hamiltonian (red dots). The mode-space method is used to construct the band structure in an energy window of interest. Here the energy window includes edge states as well as a few bulk bands. As the Fermi level lies inside the bulk gap, carrier transport takes place through the dissipationless edge bands. By shifting the Fermi level to the bulk bands, bulk states also contribute to the current. The shift in the Fermi level from edge states to the bulk states can result in scattering modulation, which is one of the switching mechanisms proposed for a TI field effect transistor [12].

The Fermi level can be modulated using a gate, as shown in Fig. 1(c). The LDoS (local density of states) taken from the middle of the channel of a TI subjected to a gate voltage in the ballistic limit is shown in Fig. 1 (d). The source-drain bias is 0.05 V. The shaded area in Fig. 1(d) represents the Fermi window. As the gate voltage increases, the bands move down and at $V_G = 0.4$ V, the entire Fermi window is covered by the protected edge states. In Fig. 1(e), it is shown that there is a noticeable edge localization of the wavefunction for the states in the bulk gap. However, the wavefunction associated with a state outside the bulk gap is not localized at the edges.

The LDoS across the width of ribbon at energy of −0.03 eV for $V_G =$ 0.4 V is denoted in Fig. 1(f). In the absence of electron phonon interactions, the state is fully localized at the edges. However, as the electron phonon scattering is taken into account, the broadening of the bulk states into the bulk gap results in considerably higher contribution of the bulk atoms to the LDoS of the considered Fermi window (Fig. 1 (g)). It is clear from Fig. 1(f) that even a deformation potential of 16 eV for acoustic phonon scattering destroys the edge localization and leads to strong degradation of the current as shown in Fig. 1(h). As the degradation is not merely a product of inter-edge scattering, increasing

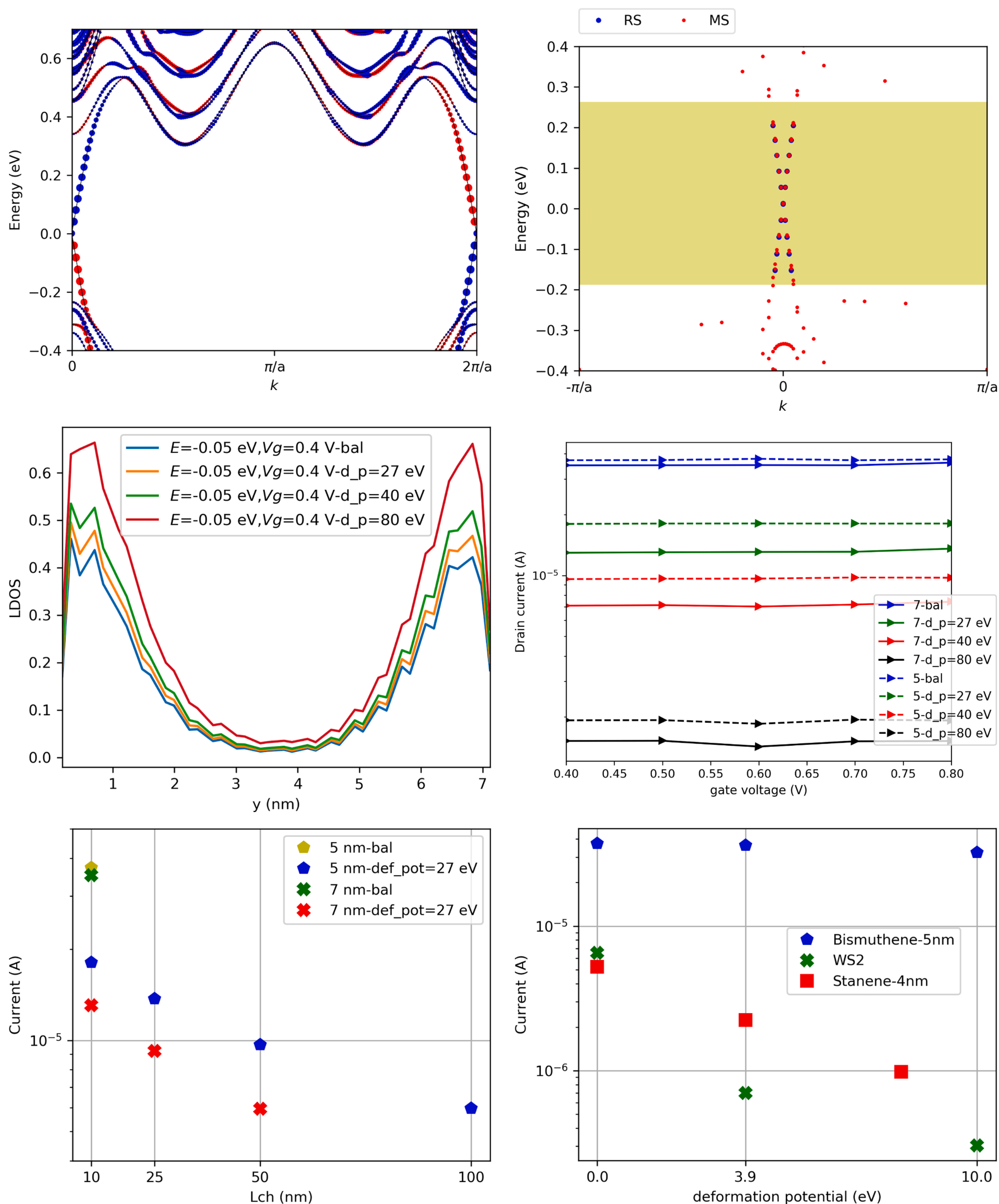

Fig. 2. (a) The spin-resolved energy band structure projected on the edge atoms of 7 nm wide zigzag bismuthene nanoribbon with H edge passivation. (b) The band structure in a target energy window calculated by RS and MS Hamiltonians. (c) LDOS across the ribbon at $E = -0.05$ eV for the ribbon under gate voltage. Different strength of electron-phonon coupling are compared by considering different deformation potentials as well as the ballistic limit (bal). (d) IV curves for ZZ bismuthene ribbons of widths 5 nm (5) and 7 nm (7) for several deformation potential values. The length of all the structures is 24 nm. (e) The current for different channel lengths. (f) The on-current obtained for bismuthene, stanene and WS2 with the same structure as a function of the deformation potential (Lch = 10 nm).

the width of the ribbon will not significantly improve the transport properties.

Fig. 2(a) and (b) illustrate the energy band structure of a 7 nm wide bismuthene zigzag nanoribbon, calculated by the real-space and mode-space Hamiltonians, respectively. The energy window of interest only contains the edge bands to gain an insight into the effect of phonon scattering on the topological protection. Furthermore, by tunning the Fermi level and the drain bias the bulk states will not participate in the transport, due to the large bulk gap. A source-drain bias of 0.2 V is considered here. Fig. 2(c) demonstrates that even a deformation potential as large as 40 eV will not destroy the edge localization.

The IV curves for the TI under gate voltage for different deformation potentials are presented in Fig. 2(d). The total length of the structure is 24 nm, unless mentioned otherwise. As the deformation potential increases to 40 eV, the drop in current is not as significant as that calculated for the stanene case. However, if the deformation potential is set to 80 eV, the current declines by an order of magnitude. The IV curves for a bismuthene nanoribbon with a width of 5 nm are also plotted in Fig. 2 (d). It is apparent that even for a smaller ribbon width, there is similar immunity to backscattering. Additionally, the current dependence on channel length (Lch) for the deformation potential of 27 eV is shown in Fig. 2(e). For Lch = 100 nm, the drop in current is smaller than one order of magnitude. Moreover, the on current as a function of the deformation potential is plotted for the same structure based on different channel materials (stanene, bismuthene and WS2 monolayers in H-phase) in Fig. 2(f). WS2 monolayer in H-phase is a topologically trivial material. Furthermore, it is made conductive by introducing doping in our simulations (3e20/cm^{-3} donor density). All the other parameters (i.e. structural and scattering parameters) are set to be the same as those of stanene and bismuthene ribbons in our simulations. This allows us to compare the dissipative transport in two TIs and topologically trivial WS2. A deformation potential as small as 3.9 eV results in a current degradation in stanene and WS2. However, the current in bismuthene is almost unchanged, supporting the idea of prohibited backscattering.

4. Conclusions

We observed that electron–phonon interactions can result in the degradation of the protected transport in a topological insulator. In stanene with a small bulk gap of 0.17 eV, electron–phonon coupling results in the extension of the bulk states into the bulk gap. Therefore, the edge localization of the states within the bulk gap is destroyed by a deformation potential as small as 16 eV. On the other hand, if we only consider the transport through the protected states of bismuthene (bulk gap $\sim$ 0.5 eV), a higher immunity to the electron–phonon scattering is obtained. The current degradation due to a deformation potential of 27 eV at a higher drain-source bias is improved significantly compared to that of stanene.

Declaration of Competing Interest

The authors declare that they have no known competing financial interests or personal relationships that could have appeared to influence the work reported in this paper.

Data availability

The data presented in this study are contained within the article and are available on reasonable request from the corresponding author.

Acknowledgements

The resources and services used in this work were in part provided by the VSC (Flemish Supercomputer Center), funded by the Research Foundation – Flanders (FWO) and the Flemish Government.

References

[1] Hasan MZ, Kane CL. Colloquium: topological insulators. Rev Mod Phys 2010;82(4): 3045–67.
[2] Bansil A, Lin H, Das T. Colloquium: Topological band theory. Rev Mod Phys 2016; 88(2):021004.
[3] Tiwari S, Van de Put ML, Sorée B, Vandenberghe WG. Carrier transport in two-dimensional topological insulator nanoribbons in the presence of vacancy defects. 2D Materials 2019;6(2):025011.
[4] Pezo A, Focassio B, Schleder GR, Costa M, Lewenkopf C, Fazzio A. Disorder effects of vacancies on the electronic transport properties of realistic topological insulator nanoribbons: The case of bismuthene. Phys Rev Mater 2021;5(1):014204.
[5] Konig M, Wiedmann S, Brune C, Roth A, Buhmann H, et al. Quantum spin Hall insulator state in HgTe quantum wells. Science 2007;318(5851):766–70.
[6] Wu S, Fatemi V, Gibson QD, Watanabe K, Taniguchi T, et al. Observation of the quantum spin Hall effect up to 100 kelvin in a monolayer crystal. Science 2018;359 (6371):76–9.
[7] Vannucci L, Olsen T, Thygesen KS. Conductance of quantum spin Hall edge states from first principles: The critical role of magnetic impurities and inter-edge scattering. Phys Rev B 2020;101(15):155404.
[8] Afzalian A, Pourtois G. Atomos: An atomistic modelling solver for dissipative dft transport in ultra-scaled hfs2 and black phosphorus mosfets. In 2019 International Conference on Simulation of Semiconductor Processes and Devices (SISPAD). pp. 1–4, 2019.
[9] Afzalian A. Ab initio perspective of ultra-scaled CMOS from 2d material fundamentals to dynamically doped transistors. NPJ 2D Mater Appl 2021;5(1):pp.
[10] Afzalian A, Huang J, Ilatikhameneh H, Charles J, Lemus D, Bermeo Lopez J, et al. Mode space tight binding model for ultra-fast simulations of III-V nanowire MOSFETs and heterojunction TFETs. In: 2015 International Workshop on Computational Electronics (IWCE). IEEE; 2015. p. 1–3.
[11] Afzalian A, Vasen T, Ramvall P, Shen T-M, Wu J, Passlack M. Physics and performance of III-V nanowire broken-gap heterojunction TFETs using an efficient tight-binding mode-space NEGF model enabling million-atom nanowire simulations. J Phys Condens Matter 2018;30(25):254002. https://doi.org/10.1088/1361-648X/aac156. 16pp.
[12] Vandenberghe W, Fischetti M. Imperfect two-dimensional topological insulator field-effect transistors. Nat Commun 2017;8(1):1–8.
[13] Ozaki T. Variationally optimized atomic orbitals for large-scale electronic structures. Phys Rev B 2003;67(15):155108.
[14] Kotaka H, Ishii F, Saito M. Rashba effect on the structure of the Bi one-bilayer film: Fully relativistic first-principles calculation. Jpn J Appl Phys 2013;52(3R):035204.
[15] Afzalian A. Computationally efficient self-consistent born approximation treatments of phonon scattering for coupled-mode space non-equilibrium Green's function. J Appl Phys 2011;110(9):094517.
[16] Afzalian A, Doornbos G, Shen T-M, Passlack M, Wu J. A High-Performance InAs/GaSb Core-Shell Nanowire Line-Tunneling TFET: An Atomistic Mode-Space NEGF Study. IEEE J Electron Dev Soc 2019;7:88–99.
[17] Vandenberghe W, Fischetti M. Calculation of room temperature conductivity and mobility in tin-based topological insulator nanoribbons. J Appl Phys 2014;116(17): 173707.
[18] Afzalian A, Akhoundi E, Gaddemane G, Duflou R, Houssa M. Advanced DFT–NEGF Transport Techniques for Novel 2-D Material and Device Exploration Including HfS2/WSe2 van der Waals Heterojunction TFET and WTe2/WS2 Metal/Semiconductor Contact. IEEE Trans Electron Devices 2021;68(11):5372–9. https://doi.org/10.1109/TED.2021.3078412.